

Soliton motion in skyrmion chains: Stabilization and guidance by nanoengineered pinningN. P. Vizarim ¹, J. C. Bellizotti Souza ², C. J. O. Reichhardt,³ C. Reichhardt,³
M. V. Milošević,^{4,5,6} and P. A. Venegas²¹*POSMAT - Programa de Pós-Graduação em Ciência e Tecnologia de Materiais, Faculdade de Ciências, Universidade Estadual Paulista - UNESP, Bauru, SP, CP 473, 17033-360, Brazil*²*Departamento de Física, Faculdade de Ciências, Unesp-Universidade Estadual Paulista, Bauru, SP, CP 473, 17033-360, Brazil*³*Theoretical Division and Center for Nonlinear Studies, Los Alamos National Laboratory, Los Alamos, New Mexico 87545, USA*⁴*NANOLab Center of Excellence & Department of Physics, University of Antwerp, Groenenborgerlaan 171, B-2020 Antwerp, Belgium*⁵*Department of Physics, University of Antwerp, Groenenborgerlaan 171, 2020 Antwerp, Belgium*⁶*Instituto de Física, Universidade Federal de Mato Grosso, 78060-900 Cuiabá, Mato Grosso, Brazil*

(Received 22 February 2022; revised 19 May 2022; accepted 8 June 2022; published 16 June 2022)

Using a particle-based model we examine the depinning motion of solitons in skyrmion chains in quasi-one-dimensional (1D) and two-dimensional (2D) systems containing embedded 1D interfaces. The solitons take the form of a particle or hole in a commensurate chain of skyrmions. Under an applied drive, just above a critical depinning threshold, the soliton moves with a skyrmion Hall angle of zero. For higher drives, the entire chain depins, and in a 2D system we observe that both the solitons and chain move at zero skyrmion Hall angle and then transition to a finite skyrmion Hall angle as the drive increases. In a 2D system with a 1D interface that is at an angle to the driving direction, there can be a reversal of the sign of the skyrmion Hall angle from positive to negative. Our results suggest that solitons in skyrmion systems could be used as information carriers in racetrack geometries that would avoid the drawbacks of finite skyrmion Hall angles. The soliton states become mobile at significantly lower drives than the depinning transition of the skyrmion chains themselves.

DOI: [10.1103/PhysRevB.105.224409](https://doi.org/10.1103/PhysRevB.105.224409)**I. INTRODUCTION**

Solitons are a well-known concept in physics for describing a nonlinear wave, also called a solitary wave, that emerges with unchanged shape and speed from a collision with a similar pulse [1]. After Zabuski and Kruskal, as part of their investigation of plasma waves [2], coined the term “soliton” due to the novel properties of these solitary waves, many other branches of science including applied mathematics [3], chemistry [4,5], and biology [6–8] proved to be fertile ground for soliton physics. While solitons are related to several important phenomena in science, such as thermal and electrical conductivity, one of the areas most impacted by the soliton concept was optics. Soliton studies greatly enhanced the technology of optical fibers [9,10], photorefractive crystals [11], and optical media [12]. Most recent studies of solitons appear primarily in optics (light waves) and matter waves.

In magnetism, the nonlinearity of the spin dynamics produces topologically nontrivial magnetic structures [13], including a rich variety of solitons, such as: One-dimensional solitons describing the motion of domain walls [14]; two-dimensional magnetic vortices [15]; magnon drops [16]; and also the two-dimensional topological solitons called skyrmions [17]. Although it is well known that skyrmions are a type of soliton, we show here that the collective motion of a chain of skyrmions can also produce a soliton on a different length scale.

Skyrmions are spin textures pointing in all directions that can be mapped onto a wrapping of a sphere, forming a topo-

logically stable object [18]. One of their most interesting features is that they can be set into motion by the application of a spin polarized current [19–23]. In the presence of external driving, skyrmions can exhibit a depinning threshold and obey nonlinear velocity-force relations [20,22–25]. There is great interest in using skyrmions as information carriers for memory and logic devices [26,27] as well as in spintronics [28] due to their stability and the low currents required to set them into motion. Application of skyrmions in actual devices will require a better understanding of their behavior, dynamics, and how to control their motion.

A key aspect of skyrmions that distinguishes them from other overdamped particles is the presence of a nondissipative component or Magnus term in their equation of motion [18,22,23,27,29]. The Magnus term produces a skyrmion velocity component perpendicular to the net force on the skyrmion, and it has been proposed that the Magnus term is responsible for the reduced depinning threshold exhibited by skyrmions [18,22,27]. In the absence of defects in the sample, an applied external drive combined with the Magnus term causes the skyrmion to move at an angle with respect to the driving direction that is called the intrinsic skyrmion Hall angle θ_{sk}^{int} [22,30,31]. The magnitude of this angle increases as the ratio of the Magnus term to the damping term is increased. Experimentally, skyrmion Hall angles have been observed that span the range from a few degrees up to very large angles, depending on the system parameters and the size of the skyrmions [31–33]. The skyrmion Hall angle deflection is a serious problem for the realization of skyrmion-based devices

since the skyrmion can go out of track and be annihilated at the edges of the sample [27,34].

Recently, it was shown that the skyrmion Hall angle can be manipulated by introducing periodic pinning [35–40]. As the external drive is increased, the skyrmion Hall angle becomes quantized due to directional locking effects very similar to those found in superconducting vortices [41] or colloidal assemblies [42–44] driven over a periodic substrate under a rotating external drive. In the case of skyrmions, the direction of the external drive remains fixed, but as the magnitude of the drive increases, the velocity dependence of the skyrmion Hall angle causes a change in the direction of skyrmion motion. On a locking step, the skyrmion Hall angle remains constant as the magnitude of the drive is varied, while changes in the skyrmion Hall angles are associated with dips or cusps in the velocity-force curves. This behavior provides a mechanism for controlling the skyrmion motion in a given sample, since a fine adjustment in the external driving can produce a large change in the skyrmion direction of motion. Several distinct methods have been proposed for controlling the skyrmion motion, including periodic pinning [35,38,39,45,46], ratchet effects [37,47–52], interface guided motion [53,54], strain gradients [55], magnetic field gradients [56–58], temperature gradients [59,60], 1D potential wells [61,62], nanotracks [63–66], and skyrmion-vortex systems in a ferromagnet-superconductor heterostructure [67].

Commensurability effects are very important in determining the collective behavior of skyrmions under the influence of periodic pinning. When the number of skyrmions N_{sk} is an integer multiple or rational fraction of the number of substrate minima N_p , we say that the system is commensurate. Extensive studies of commensurability effects have shown that they are associated with distinctive behavior in many systems, including superconducting vortices [68–70], colloidal particles [71], Wigner crystals [72], and vortices in Bose-Einstein condensates [73,74]. Much less work has been done on commensurability effects in skyrmion systems [75,76]. Recently, Reichhardt *et al.* [76] investigated commensuration effects for skyrmions in periodic pinning and found that the skyrmion Hall angle is nonmonotonic, dropping to zero at commensurate states and returning to a finite value for incommensurate states.

Solitons often appear in commensurate-incommensurate systems that are near but not in a commensurate state. Here, there is an ordered lattice containing interstitials or vacancies that behave like kinks or antikinks. Under an applied drive, these kink objects depin prior to the ordered portions of the lattice, resulting in a two-step depinning transition in which interstitials or kinks move in the driving direction and vacancies or antikinks move in the opposite direction. The classic example of a system exhibiting this behavior is the Frenkel-Kontorova model [77–79]. Kink dynamics were imaged directly in colloidal experiments for 2D periodic substrates just above and below the 1:1 commensurate conditions [80], while numerical studies of the same system showed a multistep depinning process involving kinks and antikinks [81]. Motion of kinks on periodic substrates has also been studied in 1D cold atom systems [82], 1D and 2D frictional systems [83,84], and other systems near commensuration such as superconducting vortices in periodic pinning arrays [85].

Kink motion should also be possible in skyrmion chains near commensurate conditions; however, due to the nondissipative Magnus term, such kinks would have different dynamics than previously studied kinks. Most kink systems have overdamped or underdamped dynamics and the interstitial solitons move in the same direction as the applied drive. In a skyrmion system, the Magnus term can cause the kink to move at an angle to the driving direction. Soliton motion in skyrmion chains is of interest since the solitons themselves, rather than the skyrmions, could serve as information carriers. This would be particularly relevant if kinks move along the driving direction under drives much lower than those that would be needed to translate individual skyrmions or chains of skyrmions over long distances.

In this paper, we investigate the skyrmion collective behavior just outside of a commensurate filling for $N_{sk} = N_p + 1$ or $N_{sk} = N_p - 1$. We use a heterogeneous pinning lattice containing a line of weaker pinning potentials that serve as a guide for the skyrmion motion. We apply an external dc drive to the sample and neglect thermal effects. A soliton in a skyrmion chain, formed by an interstitial skyrmion for $N_{sk} = N_p + 1$ or a vacancy for $N_{sk} = N_p - 1$, can be set into motion by the external drive. The interstitial skyrmion moves parallel to the applied drive and the vacancy moves antiparallel to the applied drive, but both have a zero skyrmion Hall angle, which is of interest for applications. We show that the line of weak pinning potentials can guide the soliton motion even to the point of causing the soliton to move in the direction $-\theta_{sk}^{int}$, opposite to the intrinsic skyrmion Hall angle. We find a multiple step depinning process in which the soliton depins first, followed next by the depinning of the skyrmion chain along the weak pinning line, and finally the depinning of the entire skyrmion assembly in the direction transverse to the drive. This opens a novel method for precise control of skyrmion motion.

II. SIMULATION

We simulate the collective behavior of N_{sk} skyrmions interacting with N_p attractive pinning centers in a $L_y \times L_x$ two-dimensional box with periodic boundary conditions in both the x and y directions, as illustrated in Fig. 1. The skyrmion density is $n_{sk} = N_{sk}/L_y L_x$ and the pinning density is $n_p = N_p/L_y L_x$. The simulations are performed just outside the commensuration ratio $N_{sk}/N_p = 1$ for either an interstitial skyrmion ($N_{sk} = N_p + 1$) or a vacancy ($N_{sk} = N_p - 1$). Initially we consider the simplest quasi-one-dimensional (1D) case where the skyrmions are confined in a line of Gaussian pinning sites and by repulsive barrier walls located at $y = 0$ and $y = L_y$, as illustrated in Fig. 1(a). We next work with a sample containing no repulsive barrier walls where there is a square lattice of pinning centers bisected by a line of weaker pinning potentials, as shown in Fig. 1(b). The weak pinning line is aligned with the driving direction in most of this paper, but we also consider the case where the weak pinning is at 45° to the driving direction.

The skyrmion dynamics is governed by the following particle based equation of motion [86]:

$$\alpha_d \mathbf{v}_i + \alpha_m \hat{z} \times \mathbf{v}_i = \mathbf{F}_i^{ss} + \mathbf{F}_i^p + \mathbf{F}_i^W + \mathbf{F}^D. \quad (1)$$

The first term on the left-hand side represents the damping that arises from the spin precession and dissipation

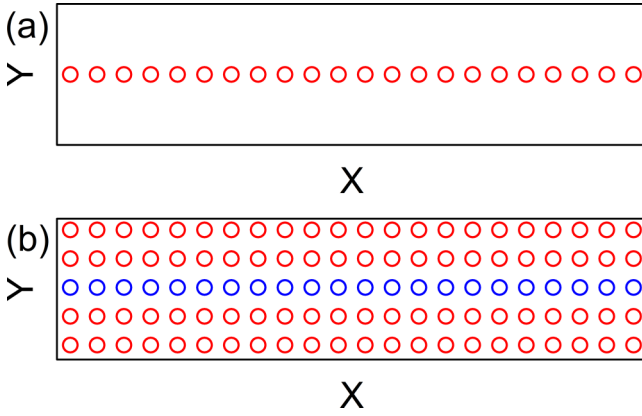


FIG. 1. Illustration of the samples used in this paper. (a) The quasi-1D system where the skyrmion motion is confined to a line of Gaussian pinning potentials (circles) and by repulsive barriers at $y = 0$ and $y = L_y$. (b) The 2D system with a square array of pinning centers and no repulsive barriers. All pinning sites are modeled using Gaussian pinning potentials. Red circles indicate stronger pinning centers and the blue circles are the weaker pinning potentials.

of electrons in the skyrmion core, where α_d is the damping constant. The second term on the left-hand side is the Magnus force, where α_m is the Magnus constant. The Magnus force is oriented perpendicular to the skyrmion velocity. The skyrmion-skyrmion repulsive interaction is $\mathbf{F}_i^{ss} = \sum_j^{N_{sk}} K_1(r_{ij}/\xi)\hat{\mathbf{r}}_{ij}$, where the screening length ξ is set to $\xi = 1.0$ in dimensionless units, $r_{ij} = |\mathbf{r}_i - \mathbf{r}_j|$ is the distance between skyrmions i and j , and $\hat{\mathbf{r}}_{ij} = (\mathbf{r}_i - \mathbf{r}_j)/r_{ij}$. For better computational efficiency, we cut off the exponentially decaying skyrmion-skyrmion interaction beyond $r_{ij} = 6.0$. We model the interaction between the skyrmions and the pinning centers using the Gaussian form $U_p = -C_p e^{-(r_{ip}/a_p)^2}$, where C_p is the strength of the pinning potential. Thus, the skyrmion-pinning interaction is given by $\mathbf{F}_i^p = -\nabla U_p = F_p r_{ip} e^{-(r_{ip}/a_p)^2} \hat{\mathbf{r}}_{ip}$, where $F_p = 2C_p/a_p^2$, r_{ip} is the distance between skyrmion i and pinning center p , and a_p is the pinning center radius. In this paper we use two types of pinning centers: Strong pinning centers with $C_p = 1.0$ and weak pinning centers with $C_p = 0.15$. In both cases the pinning radius is fixed to $a_p = 0.3$. The value of a_p was chosen so that the pinning site is small enough to trap only one skyrmion per site. We cut off this interaction beyond $r_{ip} = 2.0$ for computational efficiency. The third term on the right-hand side, \mathbf{F}_i^W , represents the force exerted by the repulsive barrier walls. In the presence of the barrier walls, the skyrmion behavior is similar to what would be observed in a quasi-1D potential well. The wall potential is $U_W = U_{W_0} \cos(wy)$, where $U_{W_0} = 12.0$ and $w = 2\pi/L_y$. The strength of the barrier wall was adjusted so that skyrmions cannot surpass this barrier even for high drives. The force exerted by the wall is given by $\mathbf{F}_i^W = -\nabla U_W = -F_W \sin(wy)$, where $F_W = 2\pi U_{W_0}/L_y$. The term $\mathbf{F}^D = F^D \hat{\mathbf{x}}$ represents the applied dc drive, which is fixed to be along the positive x direction. We increase F^D in small steps of $\delta F^D = 0.01$ and spend 2×10^5 simulation time steps at each drive increment. We measure the average velocities $\langle V_x \rangle = \langle \mathbf{v} \cdot \hat{\mathbf{x}} \rangle$ and $\langle V_y \rangle = \langle \mathbf{v} \cdot \hat{\mathbf{y}} \rangle$. We normalize all distances

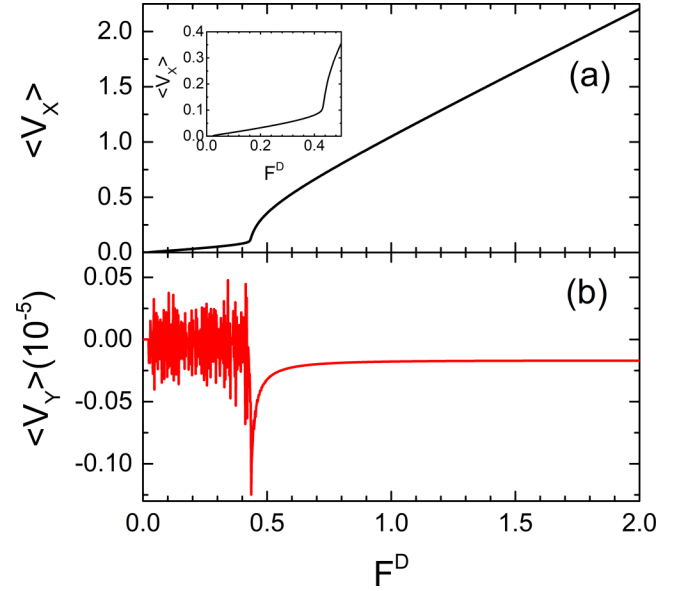


FIG. 2. (a) $\langle V_x \rangle$ and (b) $\langle V_y \rangle$ vs the external dc drive F^D for the sample illustrated in Fig. 1(a) with $N_{sk}/N_p = 1.044$, $\alpha_m/\alpha_d = 0.5$, and $\rho_p = 0.093\xi^2$. The inset of (a) shows a blowup of panel (a) over the range $0 < F^D < 0.5$.

by the screening length ξ and select the damping and Magnus constants such that $\alpha_m^2 + \alpha_d^2 = 1$.

For comparison with experiments, considering a MnSi thin film [87] with lattice constant $a \approx 0.5$ nm, the exchange energy is $J \approx 3$ meV/a, the Dzyaloshinskii-Moriya energy is $D \approx 0.3$ meV/a², and the skyrmion size is $\xi \approx 2\pi J/D \approx 30$ nm. The depinning currents would be of order 10^8 A/m² for MnSi nanowires [24]. Similar mappings of simulation parameters can be made for different materials.

III. THE QUASI-1D SYSTEM

We first consider the quasi-1D system illustrated in Fig. 1(a). In this case, repulsive barrier walls at $y = 0$ and $y = L_y$ surround an isolated line of $N_p = 22$ weak pinning centers filled with $N_{sk} = 23$ skyrmions, giving a value $N_{sk}/N_p = 1.044$ that is just outside a commensurate ratio. For this quasi-1D system we use $L_x = 36\xi$ and $L_y = 6.546\xi$. The pinning density is fixed to $\rho_p = 0.093/\xi^2$. In Fig. 2 we plot $\langle V_x \rangle$ and $\langle V_y \rangle$ as a function of the applied dc drive F^D for a system with $\alpha_m/\alpha_d = 0.5$. After the depinning at $F^D = 0.02$, there is a low-velocity regime in which $\langle V_y \rangle$ is noisy and $\langle V_x \rangle$ increases smoothly and monotonically with increasing drive. The behavior of $\langle V_x \rangle$ is highlighted in the inset of Fig. 2(a). The motion is largely confined to the x direction by the repulsive barrier walls, while the motion in the y direction is either absent or composed of small amplitude oscillations. Over the range $0.02 < F^D < 0.43$, a soliton pulse is translating along the skyrmion chain. Under application of an external drive, the initial interstitial skyrmion shown in Fig. 3(a) displaces its neighboring skyrmion from the pinning site. The neighboring skyrmion becomes the new interstitial skyrmion and the previous interstitial skyrmion is now pinned. The result is a propagation of the location of the interstitial skyrmion along the chain in the $+x$ direction, as illustrated in Fig. 3(b).

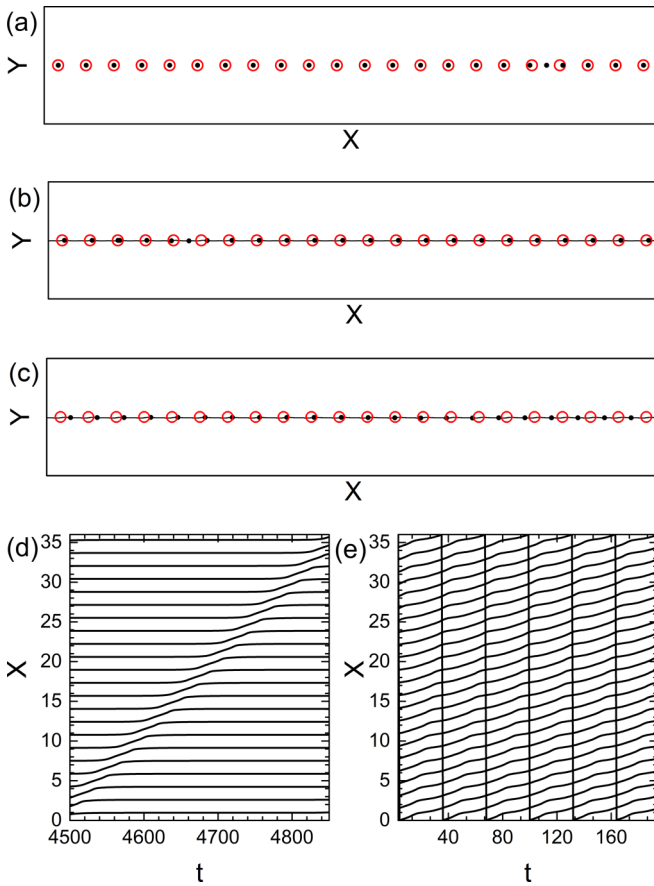


FIG. 3. [(a), (b), (c)] Pinning site positions (red circles) and the skyrmion trajectory (black lines) for a sample with $N_{sk} = 23$, $N_p = 22$, $N_{sk}/N_p = 1.044$, $\alpha_m/\alpha_d = 0.5$, $C_p = 0.15$, and $\rho_p = 0.093/\xi^2$. (a) At $F^D = 0.01$, the skyrmions are static in the pinned phase. The incommensuration produces a deformation in the lattice in the form of an interstitial skyrmion. (b) At $F^D = 0.3$, the interstitial skyrmion moves as a soliton by hopping from site to site with slow average velocity. (c) At $F^D = 1.0$, all of the skyrmions are flowing simultaneously at a higher velocity. [(d), (e)] Skyrmion positions as a function of time. (d) For $F^D = 0.3$ as in panel (b), a soliton pulse propagates through the sample. (e) For $F^D = 1.0$, as in panel (c), all of the skyrmions are flowing in unison.

For $F^D > 0.43$, all of the skyrmions depin and begin to move collectively, producing a spike in the velocity-force curve as shown in Fig. 2(a). Due to the orderliness of the motion, the velocity component $\langle V_y \rangle$ drops to zero. The soliton or kink motion occurs because the additional skyrmion creates a local density peak that propagates as the drive is applied. In this way, the local density pulse moves much more rapidly through the system than the individual skyrmions. Since the soliton is not associated with a single continuously moving particle, it does not have the same effective equation of motion as the skyrmions, and in particular it does not exhibit the skyrmion Hall effect associated with a continuously moving skyrmion. Since the soliton can be pinned or moved, it could also be employed as an information carrier, but with the absence of a finite Hall angle, which may be useful for skyrmion-based devices. Moreover, the ability of the soliton to depin at lower drives than the individual skyrmions trapped at the pins is

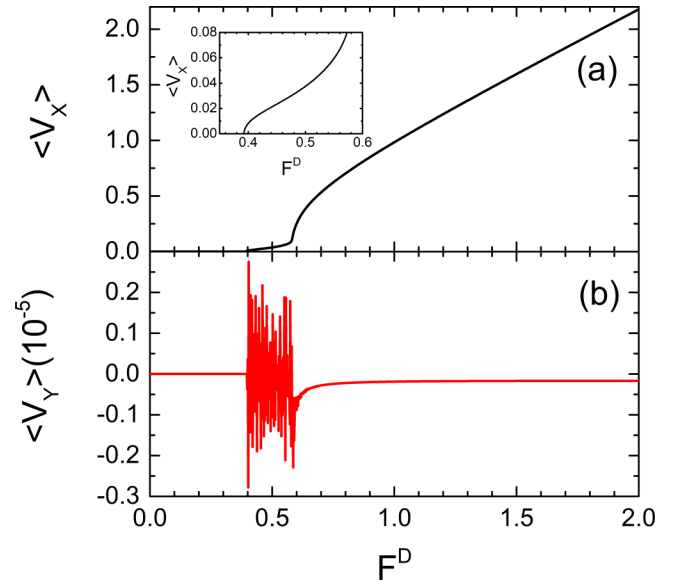


FIG. 4. (a) $\langle V_x \rangle$ and (b) $\langle V_y \rangle$ vs F^D for the sample illustrated in Fig. 1(a) with $N_{sk}/N_p = 0.96$, $\alpha_m/\alpha_d = 0.5$ and $\rho_p = 0.093/\xi^2$. The inset of (a) shows a blowup of panel (a) over the range $0.35 < F^D < 0.6$.

due to the interactions between skyrmions. The denser the skyrmion assembly becomes, the lower the drive required to move the soliton becomes. Additionally, as the drive increases, the soliton moves faster but also gets effectively larger, forming an incommensurate chain of skyrmions that depin slightly below the depinning force of that found for a commensurate skyrmion chain.

It is difficult to see the differences in motion between Figs. 3(b) and 3(c) from the overlapping skyrmion trajectories, so in Figs. 3(d) and 3(e) we plot the position of each skyrmion as a function of time. In Fig. 3(d), the system from Fig. 3(b) at $F^D = 0.3$ contains a clearly propagating soliton pulse. In contrast, Fig. 3(e) shows the system from Fig. 3(c) at $F^D = 1.0$, where all of skyrmions are moving coherently as a crystal and the soliton motion is lost.

In Fig. 4 we plot $\langle V_x \rangle$ and $\langle V_y \rangle$ versus F^D for a system with $N_{sk} = 21$, $N_p = 22$, $N_{sk}/N_p = 0.96$, and $\alpha_m/\alpha_d = 0.5$. The depinning falls at $F^D = 0.39$, a higher value than that found in Fig. 2 due to the reduced density of skyrmions in the sample. Just above depinning, there is a regime of low average velocity similar to that observed in Fig. 2; however, the dynamics is different. As is shown in Fig. 5(a), there is a vacancy due to the incommensurate ratio between the skyrmions and the pinning centers. Here, the vacancy forms an antikink soliton that can be viewed as a suppression of the local density. This vacancy moves through the sample in the $-x$ direction as the neighboring pinned skyrmion depins and fills in the vacancy, turning its previous pinning site into a new vacancy. A repetition of this process occurs over the range $0.39 < F^D < 0.58$, where $\langle V_y \rangle$ is noisy and $\langle V_x \rangle$ increases smoothly with increasing F^D as highlighted in the inset of Fig. 4(a). The soliton can be detected experimentally in the same way as skyrmions by looking for the variation in the skyrmion spacing. For $F^D > 0.58$, all of the skyrmions depin

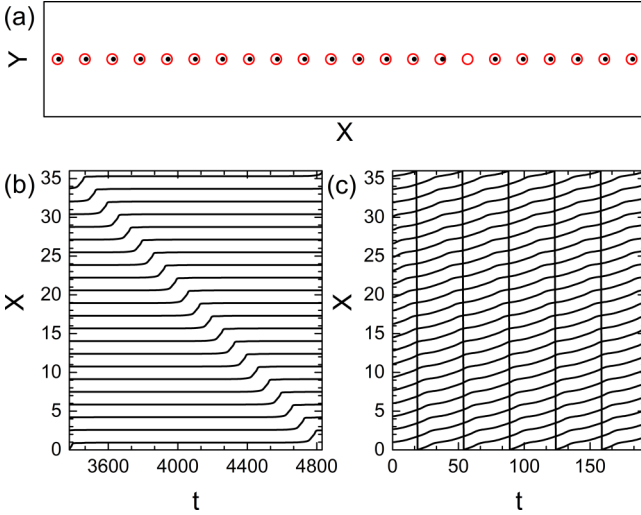


FIG. 5. (a) Pinning site positions (red circles) and the skyrmion trajectory (black lines) for a sample with $N_{sk} = 21$, $N_p = 22$, $N_{sk}/N_p = 0.96$, $\alpha_m/\alpha_d = 0.5$, $C_p = 0.15$, and $\rho_p = 0.093/\xi^2$. (a) At $F^D = 0.3$, the skyrmions are static in the pinned phase. The incommensuration produces a deformation in the lattice in the form of a vacant pinning site. [(b), (c)] Skyrmion positions as a function of time. (b) At $F^D = 0.45$, a soliton pulse propagates in the $-x$ direction through the sample. (c) At $F^D = 1.0$, all of the skyrmions are flowing in an ordered lattice.

and flow through the sample as a moving lattice with an average velocity component $\langle V_x \rangle$ that increases rapidly with increasing F^D and with $\langle V_y \rangle \approx 0$. The plot of the skyrmion positions versus time in Fig. 5(b) at $F^D = 0.45$ shows the backwards propagation of the soliton pulse, while a similar plot in Fig. 5(c) at $F^D = 1.0$ indicates that all of the skyrmions are moving in unison through the system and the soliton pulse has been destroyed.

IV. THE 2D SYSTEM

We next turn to a fully two-dimensional sample containing no repulsive barrier walls, so that $F_W = 0$. The sample contains a square array of $N_p = 110$ pinning sites, most of which have a strong $C_p = 1.0$. As illustrated in Fig. 1(b), there is a central line of weak pinning centers with $C_p = 0.15$, which serve as a channel to guide the skyrmion motion. The pinning density in this section is fixed to $\rho_p = 0.373/\xi^2$ and we set $L_x = 36\xi$ and $L_y = 8.2\xi$.

In Fig. 6(a) we plot $\langle V_x \rangle$ and $\langle V_y \rangle$ as a function of the applied dc drive F^D for a system with $N_{sk} = 111$, $N_p = 110$, $N_{sk}/N_p = 1.01$, and $\alpha_m/\alpha_d = 1.0$, while in Fig. 6(b) we show the corresponding skyrmion Hall angle θ_{sk} versus F^D . The skyrmion dynamics is no longer locked in the x direction, resulting in a diverse array of dynamic phases possible. For $F^D \leq 0.11$ the system is in the pinned phase, as illustrated in Fig. 7(a). The interstitial skyrmion is localized between four pinning centers, two of which are strong and two of which are weak. The skyrmions trapped in the weaker pinning potentials experience a greater displacement due to the neighboring interstitial skyrmion. For $0.11 < F^D < 0.41$, we find a soliton phase very similar to that shown in Fig. 2 and Fig. 3(b) for the quasi-1D system. The interstitial skyrmion displaces

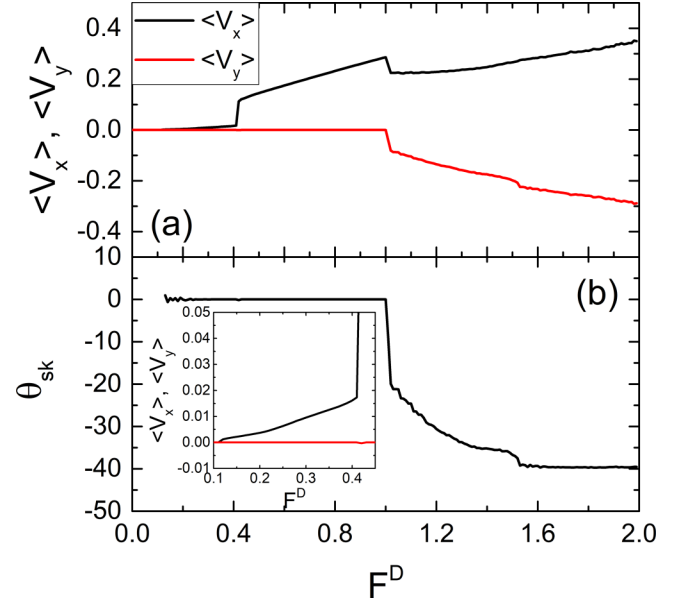


FIG. 6. (a) $\langle V_x \rangle$ (black) and $\langle V_y \rangle$ (red) vs F^D for the 2D sample illustrated in Fig. 1(b) with $N_{sk}/N_p = 1.01$, $\alpha_m/\alpha_d = 1.0$, and $\rho_p = 0.373/\xi^2$. Inset: A blowup of panel (a) over the range $0.1 < F^D < 0.45$. (b) The corresponding skyrmion Hall angle θ_{sk} versus F^D .

a skyrmion from a weak pinning site, taking its place as a pinned skyrmion and turning the formerly pinned skyrmion into the new interstitial skyrmion. This process propagates along the chain, resulting in a soliton pulse moving in the $+x$ direction. The skyrmion trajectories for this regime are illustrated in Fig. 7(b), which shows that oscillations in the y direction occur due to the combination of the skyrmion Hall angle effect and the swapping of interstitial and pinned skyrmions. For $0.41 < F^D < 1.0$, all of the skyrmions trapped in the weaker pinning potentials depin, resulting in an almost 1D motion with very small oscillations in y , as illustrated in Fig. 7(c). For $F^D > 1.0$, the skyrmions in the stronger pinning potentials also depin, resulting in a 2D motion. This motion occurs in two distinct phases that are visible in Fig. 6. In the chaotic phase, found for $1.0 < F^D < 1.53$, the skyrmion Hall angle increases irregularly in magnitude, while for $F^D > 1.53$, the skyrmion Hall angle stabilizes at $\theta_{sk} \approx -40^\circ$. If the applied drive were increased further, we expect that θ_{sk} would approach the intrinsic Hall angle, which in this case is $\theta_{sk}^{int} = \arctan(\alpha_m/\alpha_d) = -45^\circ$. The transition from 1D to 2D motion is also characterized by an increase in $\langle V_y \rangle$ and a drop in $\langle V_x \rangle$. The average skyrmion velocity is lower in the 2D motion regime since the skyrmions are flowing through the region of stronger pinning potentials, which hinder the skyrmion motion and reduce the velocity. In Fig. 7(d) we plot the skyrmion trajectories for $F^D = 1.8$, where the skyrmion Hall angle is stabilized, showing an orderly 2D motion. As in the quasi-1D system, the soliton phase is most easily identified by plotting the skyrmion positions as a function of time. In Fig. 7(e) we plot the x position of the skyrmions as a function of time for $F^D = 0.25$, where a soliton pulse propagates in the $+x$ direction. In contrast, for $F^D = 0.5$, Fig. 7(f) indicates that the pulsed motion has been destroyed and the skyrmions move as a confined chain.

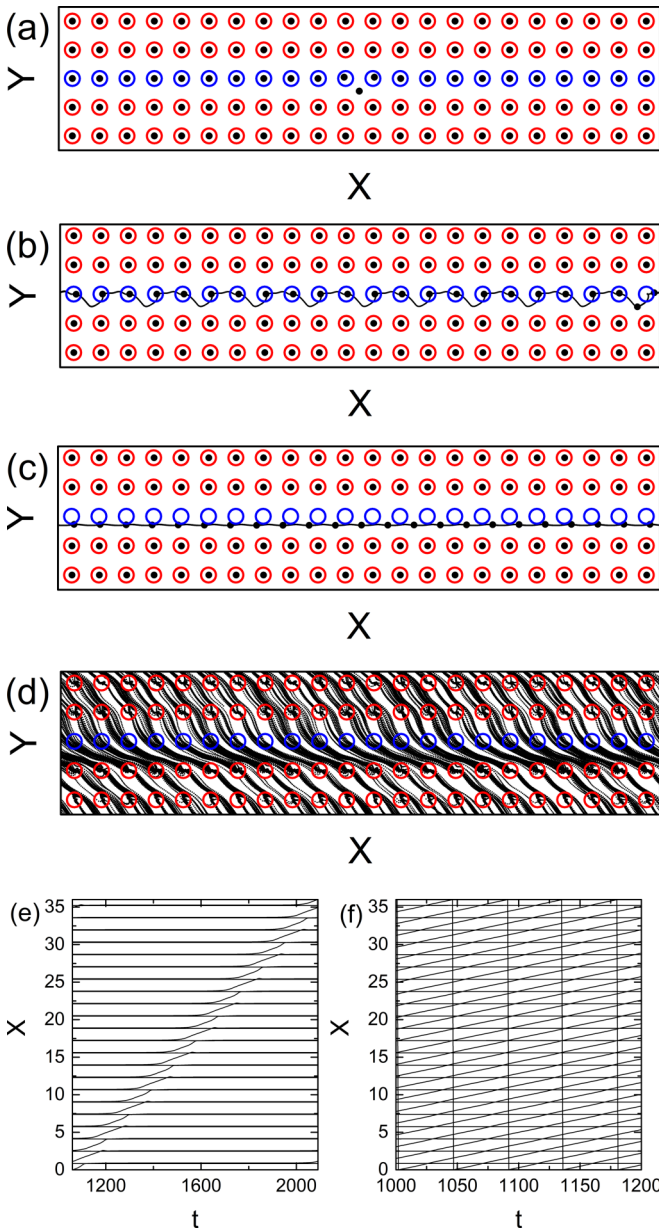


FIG. 7. [(a), (b), (c), (d)] Pinning site positions (red circles: Strong pins; blue circles: Weak pins) and the skyrmion trajectories (black lines) for a 2D sample with $N_{sk}/N_p = 1.01$, $\alpha_m/\alpha_d = 1.0$, weak pins of $C_p = 0.15$, strong pins of $C_p = 1.0$, and $\rho_p = 0.373/\xi^2$. (a) $F^D = 0$ in the ground state, where most skyrmions (black circles) are pinned and a single interstitial skyrmion is present. (b) The soliton phase at $F^D = 0.25$. (c) At $F^D = 0.5$, all of the skyrmions in the weak pinning centers depin and flow as a confined chain through the sample. (d) At $F^D = 1.8$, all of the skyrmions are depinned and flow along $\theta_{sk} = -40^\circ$. [(e), (f)] Skyrmion x positions as a function of time. (e) The soliton phase at $F^D = 0.25$ from panel (b). (f) The confined chain flow phase at $F^D = 0.5$ from panel (c), where the soliton motion is lost.

In Fig. 8(a) we plot $\langle V_x \rangle$ and $\langle V_y \rangle$ as a function of the applied dc drive F^D for a system with $N_{sk} = 109$, $N_p = 110$, $N_{sk}/N_p = 0.99$, and $\alpha_m/\alpha_d = 1.0$, while in Fig. 8(b) we show the corresponding skyrmion Hall angle θ_{sk} versus F^D . For $F^D \leq 0.24$ the system is in the pinned state, as

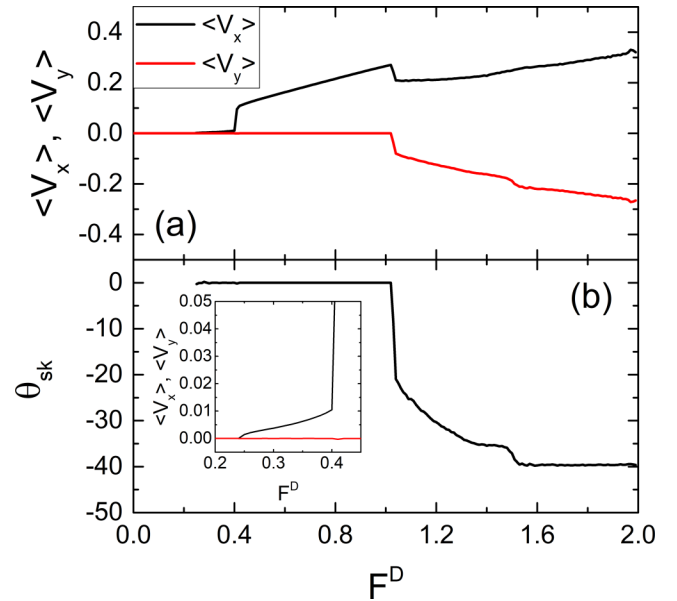


FIG. 8. (a) $\langle V_x \rangle$ (black) and $\langle V_y \rangle$ (red) vs F^D for the 2D sample from Fig. 1(b) with $N_{sk}/N_p = 0.99$, $\alpha_m/\alpha_d = 1.0$, and $\rho_p = 0.373/\xi^2$. (b) The corresponding skyrmion Hall angle θ_{sk} vs F^D . Inset: A blowup of panel (a) over the range $0.2 < F^D < 0.45$.

shown in Fig. 9(a). Due to the incommensurate ratio between the skyrmions and the pinning centers, there is a vacant pinning center, which distorts the lattice. For $0.24 < F^D < 0.4$ the system enters a soliton phase similar to that shown in Fig. 4 and Fig. 5(b) for the quasi-1D case. The vacancy is pushed in the $-x$ direction due to the hopping motion of individual skyrmions in the $+x$ direction. The trajectories in this regime are illustrated in Fig. 9(b), where small oscillations in the y direction are visible. For $0.4 < F^D < 1.02$, all of the skyrmions trapped in the weaker pinning potentials depin, resulting in an almost 1D motion with very small oscillations in y , as shown in Fig. 9(c). When $F^D > 1.02$, the skyrmions in the stronger pinning centers also depin. Similarly to what was observed in Fig. 6, Fig. 8 indicates that there are two dynamic phases for $F^D > 1.02$: A chaotic phase in the range $1.02 < F^D < 1.53$, and a more ordered phase for $F^D > 1.53$. For the latter phase, the skyrmion Hall angle again stabilizes near $\theta_{sk} \approx -40^\circ$. The similarities between the dynamics of both the interstitial and vacancy systems at high drives is expected since the difference in the skyrmion density is very low and becomes unimportant in the drive-dominated regime. In contrast, distinct behaviors arise in the soliton regime. To illustrate this, in Fig. 9(e) we plot the skyrmion x positions as a function of time at $F^D = 0.3$, where a moving soliton pulse is clearly visible. In contrast, for $F^D = 0.5$, Fig. 9(f) shows that the pulsed motion is lost.

The soliton phases for the interstitial and vacancy states have similar dynamics, but exhibit the crucial difference that the interstitial soliton moves in the $+x$ direction while the vacancy soliton moves in the $-x$ direction. This interesting behavior, which is stable over a range of external dc drives, can be harnessed in devices to allow very low external currents to propagate the soliton through the sample in a fast and controlled manner.

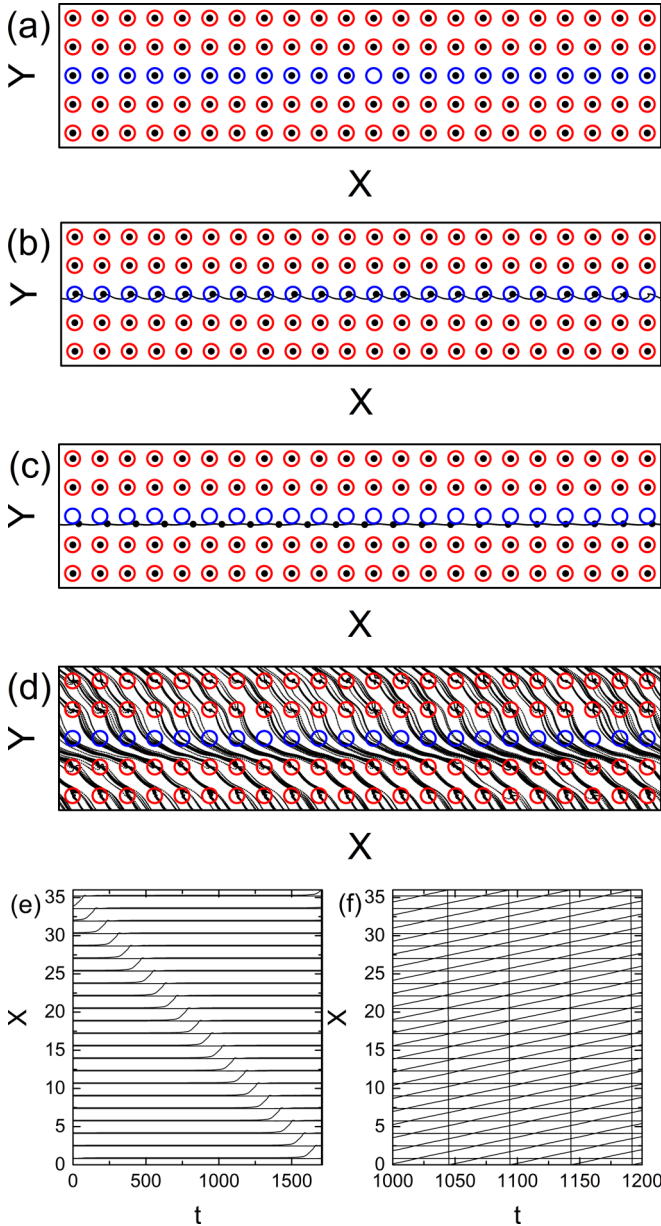


FIG. 9. [(a), (b), (c), (d)] Pinning site positions (red circles: Strong pins; blue circles: Weak pins) and the skyrmion trajectories (black lines) for a 2D sample with $N_{sk}/N_p = 0.99$, $\alpha_m/\alpha_d = 1.0$, weak pins of $C_p = 0.15$, strong pins of $C_p = 1.0$, and $\rho_p = 0.373/\xi^2$. (a) The ground state at $F^D = 0$, where all skyrmions are pinned and a single vacancy is present. (b) The soliton phase at $F^D = 0.3$. (c) At $F^D = 0.5$, all of the skyrmions in the weak pinning centers depin and flow as a chain through the sample. (d) At $F^D = 1.6$, all of the skyrmions are depinned and flow with $\theta_{sk} = -40^\circ$. [(e), (f)] Skyrmion x positions as a function of time. (e) The soliton phase at $F^D = 0.3$ from panel (b). (f) The flowing chain phase at $F^D = 0.5$ from panel (c), where the soliton motion is lost.

V. SOLITON STABILIZATION AS A FUNCTION OF α_m/α_d

We next consider the evolution of the soliton phase as α_m/α_d is varied. When α_m/α_d increases, the intrinsic skyrmion Hall angle also increases, so it is important to verify whether the soliton phase remains stable under these

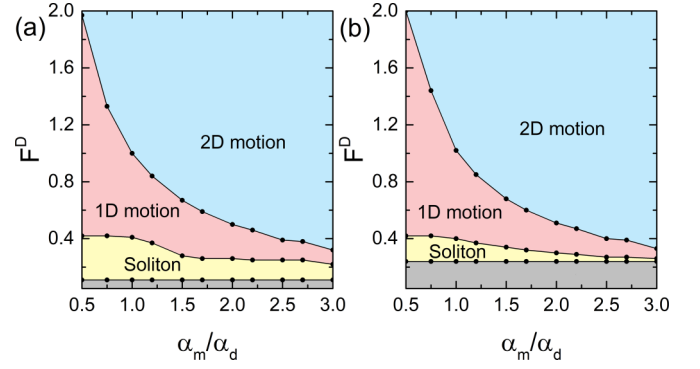


FIG. 10. Dynamic phase diagrams as a function of external dc drive F^D vs α_m/α_d for the system in Fig. 1(b) at $\rho_p = 0.373/\xi^2$ and (a) $N_{sk}/N_p = 1.01$ and (b) $N_{sk}/N_p = 0.99$. Pinned phase: Gray; soliton phase: Yellow; 1D motion: Red; 2D motion: Blue.

circumstances. We prepare two samples with fixed values of $N_{sk}/N_p = 1.01$ and $N_{sk}/N_p = 0.99$ and perform simulations for a range of values of α_m/α_d . By combining the resulting data we generate dynamic phase diagrams as a function of F^D versus α_m/α_d , shown in Fig. 10, where we identify the locations of the pinned phase, the soliton phase, 1D chain motion, and 2D motion. The pinned phase is a static state in which all pinned skyrmions remain trapped in the pinning centers and $\langle V_x \rangle = \langle V_y \rangle = 0$. In the soliton phase, the localized lattice deformation propagates through the sample. This soliton travels in the $+x$ direction when interstitial skyrmions are present and in the $-x$ direction when vacancies are present. 1D motion occurs when all of the skyrmions trapped in the weak pinning potentials depin and flow as a coherent chain in the $+x$ direction. In 2D motion, all of the skyrmions in all of the pinning sites depin and flow through the sample along both the x and y directions.

At $N_{sk}/N_p = 1.01$, Fig. 10(a) indicates that the depinning threshold is very low, producing a wider range of soliton motion compared to the system in Fig. 10(b) with $N_{sk}/N_p = 0.99$. Interstitial skyrmions are more mobile than vacancies since an interstitial skyrmion is trapped only by the caging potentials of the neighboring skyrmions and not directly by a pinning site. This lowers the depinning threshold for the interstitial system. Both systems show a transition from the soliton phase to 1D motion at roughly the same value of F^D since this transition is controlled by the strength of the weak pinning sites. Similarly, the transition line between 1D motion and 2D motion, which is controlled by the strength of the strong pinning sites, falls at similar values of F^D in both systems.

VI. EFFECT OF PINNING DENSITY

We next vary the pinning density ρ_p for $N_{sk}/N_p = \rho_{sk}/\rho_p = 1.01$ and 0.99 while fixing $\alpha_m/\alpha_d = 0.5$. When the pinning density is low, we expect that the soliton motion will vanish when the large spacing between adjacent pinning sites destroys the collective behavior. In Figs. 11(a) and 11(b) we show dynamic phase diagrams as a function of F^D versus ρ_p for both systems. Here we observe a pinned phase, a soliton phase, 1D motion, 2D motion, and an additional phase we term single skyrmion 1D motion (SK1D). In the SK1D state,

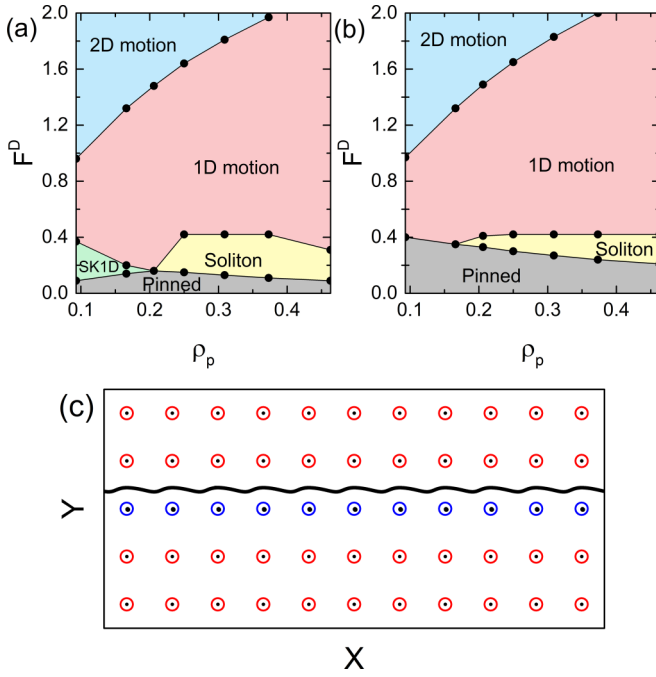


FIG. 11. [(a), (b)] Dynamic phase diagrams as a function of F^D vs pinning density ρ_p for the samples from Fig. 1(b) with $\alpha_m/\alpha_d = 0.5$, weak pinning of $C_p = 0.15$, and strong pinning of $C_p = 1.0$ for (a) $N_{sk}/N_p = 1.01$ and (b) $N_{sk}/N_p = 0.99$. Pinned phase: Gray; soliton phase: Yellow; 1D motion: Red; 2D motion: Blue; single skyrmion 1D motion (SK1D): Green. (c) Pinning site positions (red circles: Strong pins; blue circles: Weak pins) and the skyrmion trajectories (black lines) for the $N_{sk}/N_p = 1.01$ sample at $F^D = 0.2$ and $\rho_p = 0.093/\xi^2$.

the interstitial skyrmion produced by the incommensuration in the $N_{sk}/N_p = 1.01$ sample flows between the pinning centers without displacing any of the pinned skyrmions. This behavior occurs only for low pinning densities, $\rho_p < 0.206$, when the gaps between adjacent pinning sites are sufficiently large, as shown in Fig. 11(c). The SK1D phase is very similar to the previously studied motion of single skyrmions through periodic pinning lattices [35,38,45]. As the pinning density increases, the SK1D motion vanishes and is replaced by soliton motion. The gaps between the pinning centers diminish with increasing ρ_p , making it impossible for the interstitial skyrmion to move unless it exchanges places with neighboring skyrmions in a soliton-like fashion.

In the vacancy-containing sample with $N_{sk}/N_p = 0.99$, Fig. 11(b) shows that there is a monotonic decrease of the depinning threshold with increasing ρ_p . As the sample density increases, the relative strength of the skyrmion-skyrmion interactions increases compared to the pinning energy, causing a suppression of the depinning threshold. Soliton motion is completely lost for $\rho_p < 0.166$ when the large distance between adjacent pinning sites destroys the collective behavior required to propagate a skyrmion through the sample. For $\rho_p > 0.166$, the extent of the soliton phase increases with increasing pinning density, primarily due to the decrease in the depinning threshold. Both the $N_{sk}/N_p = 1.01$ and $N_{sk}/N_p = 0.99$ samples show a similar transition from 1D motion to 2D

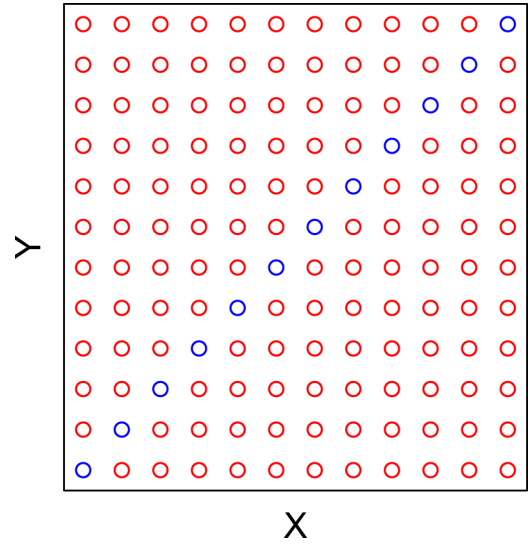


FIG. 12. Pinning site positions (red circles: Strong pins; blue circles: Weak pins) for a sample with a diagonal line of weak pinning oriented at $+45^\circ$ with respect to the x direction applied drive. The weak pins have $C_p = 0.15$, the strong pins have $C_p = 1.0$, and we set $\rho_p = 0.373/\xi^2$.

motion since this transition is dominated by the skyrmions in the strong pinning sites, which are the same in both systems.

VII. GUIDANCE OF SOLITON MOTION AND SKYRMION HALL ANGLE REVERSAL

We have shown that soliton motion through skyrmion chains can be enhanced depending on the choice of pinning density and α_m/α_d . We next ask whether it is possible to guide the soliton motion along a specific direction. When we introduced a line of weak pinning in the sample, the soliton followed this line along the $+x$ or $-x$ direction, depending on the value of N_{sk}/N_p , even though this direction is not aligned with the intrinsic Hall angle. In other words, guiding by the line of weak pinning potentials can overcome the skyrmion Hall angle. To further explore this effect, we change the skyrmion Hall angle so that it is perpendicular to the guiding line of weaker pinning potentials. As shown in Fig. 12, we place the line of weak pinning centers along $\theta_p = +45^\circ$ with respect to the driving or x direction. By selecting $\alpha_m/\alpha_d = 1.0$, we obtain an intrinsic skyrmion Hall angle of $\theta_{sk}^{\text{int}} = -45^\circ$, so that $\Delta\theta = \theta_p - \theta_{sk}^{\text{int}} = 90^\circ$. For this section we set $L_x = L_y = 19.638\xi$.

For a sample with $N_{sk}/N_p = 1.01$, we plot $\langle V_x \rangle$ and $\langle V_y \rangle$ versus F^D in Fig. 13(a) and show the corresponding skyrmion Hall angle θ_{sk} versus F^D in Fig. 13(b). When $F^D < 0.12$, the skyrmions are in the pinned phase, marked by the letter P in Fig. 13(a). As F^D increases, we observe a small and continuous increase of both velocity components, which remain equal to each other so that $\langle V_x \rangle = \langle V_y \rangle$. Here the motion is occurring at exactly $+45^\circ$ with respect to the driving direction and is following the line of weak pinning centers. An illustration of this soliton motion appears in Fig. 14(a). For $0.44 < F^D < 0.56$, the skyrmion velocity components remain equal to each other but do not change as the drive increases.

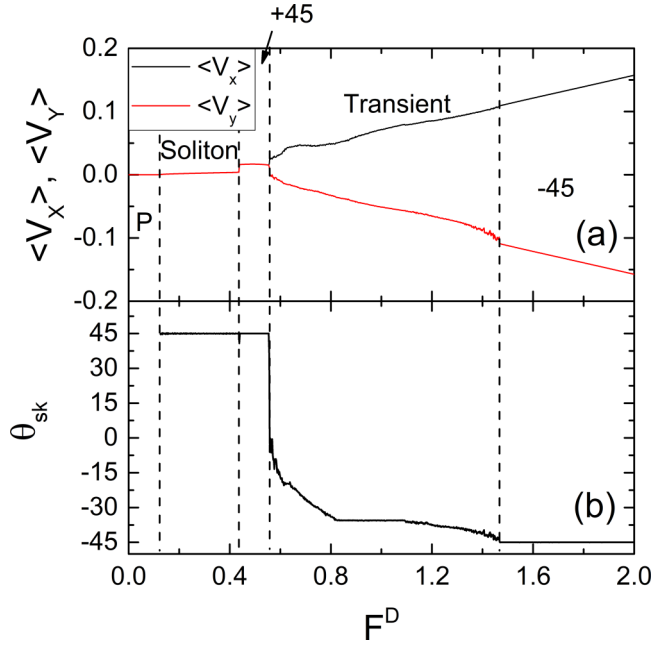


FIG. 13. (a) $\langle V_x \rangle$ (black) and $\langle V_y \rangle$ (red) vs F^D for the sample illustrated in Fig. 12(b) with $N_{sk}/N_p = 1.01$, $\alpha_m/\alpha_d = 1.0$, and $\rho_p = 0.373/\xi^2$. (b) The corresponding skymion Hall angle θ_{sk} vs F^D . P indicates the pinned phase, Soliton is the soliton phase, +45 is the phase in which the skyrmions that have depinned from the weak pinning centers flow with $\theta_{sk} = +45^\circ$, Transient is the phase in which the skymion Hall angle is reversing, and -45 is the phase in which the motion is locked to $\theta_{sk} = -45^\circ$.

In this regime, all of the skyrmions in the weak pinning sites depin and flow with $\theta_{sk} = +45^\circ$, as shown in Fig. 14(b). Note that the skyrmion flow follows a much more tortuous trajectory compared to the case shown in Fig. 7(c). This occurs due to the different orientation of the weak line of pinning potentials. There is a larger space between pinning sites along the diagonal direction, making zig-zag motion possible. For $0.56 < F^D < 1.47$ we find a broad transient phase in which the skymion Hall angle slowly changes from $\theta_{sk} = +45^\circ$ to $\theta_{sk} = -45^\circ$. Here, the skyrmions in the strong pinning sites remain pinned, but the depinned skyrmions from the weak pinning sites begin to escape from the weak pinning channel that is aligned with $\theta_{sk} = +45^\circ$ and instead start flowing along the intrinsic skymion Hall angle of $\theta_{sk}^{int} = -45^\circ$. A step in the skymion Hall angle at $\theta_{sk} = 35.6^\circ$ appears around the value $F^D = 1.0$, corresponding to the flow state illustrated in Fig. 14(c). This motion is unstable and the magnitude of the skymion Hall angle continues to increase once F^D is raised above the step region. The collective motion only becomes stable once $F^D > 1.46$, when the skyrmions flow in an orderly fashion along $\theta_{sk} = -45^\circ$, as shown in Fig. 14(d). Here, some of the skyrmions that were previously trapped in the stronger pinning centers have now depinned and serve to stabilize the flow. The depinning of the remaining skyrmions occurs only for drives higher than those considered here. Other Hall angle reversals are expected if different directions of weak line of pinning sites are used with different type of skyrmions with different values of α_m/α_d .

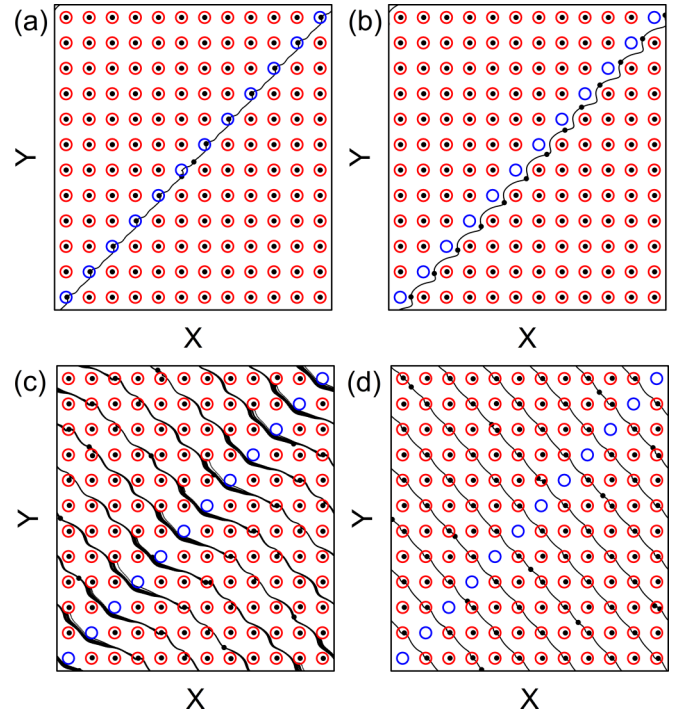


FIG. 14. Pinning site positions (red circles: Strong pins; blue circles: Weak pins) and the skymion trajectories (black lines) for a sample with $N_{sk}/N_p = 1.01$, $\alpha_m/\alpha_d = 1.0$, $\rho_p = 0.373/\xi^2$, weak pinning of $C_p = 0.15$, and strong pinning of $C_p = 1.0$. (a) $F^D = 0.25$, where a soliton flows along the line of weak pinning centers at $\theta_{sk} = +45^\circ$. (b) At $F^D = 0.5$, the skyrmions trapped at the weak pinning sites depin and flow along $\theta_{sk} = +45^\circ$. (c) $F^D = 1.0$, the transient phase, where the skymion Hall angle gradually reverses. At this stage, the skymion Hall angle is $\theta_{sk} = -35.6^\circ$. (d) At $F^D = 1.8$ the skymion Hall angle reversal is complete and the skyrmions flow along $\theta_{sk} = -45^\circ$.

VIII. DISCUSSION

Using particle-based simulations we showed that just outside commensurate states, skyrmions may exhibit a soliton phase for low drives that is of interstitial or vacancy type. We model the skyrmions as point-like rigid bodies that cannot deform or change size; however, in real materials, skyrmions may deform, change size, merge, or be annihilated. These features can change the dynamics of the soliton phase or give rise to new phenomena, which could be explored further using continuum-based simulations. Thermal fluctuations, neglected here, could also modify the behavior, such as by introducing thermal creep in the low drive regimes. We expect that the soliton phase would remain stable for a certain range of temperatures. The soliton phase can occur for other pinning site geometries, but the preferential directions of motion would be changed. For the square lattice we consider here, soliton motion is stabilized along 0° or 45° as shown in our results. For other geometries, such as a triangular pinning lattice, the soliton motion would occur along 0° , 30° , and 60° .

IX. SUMMARY

In this paper we investigated the collective behavior of skyrmions at zero temperature using a channel of weak

pinning sites inserted into a periodic lattice of strong pinning sites for slightly incommensurate fillings. We demonstrated that soliton motion can flow along the chains of weak pinning sites. The system displays two types of soliton motion: (i) motion in the direction of drive for an interstitial soliton, and (ii) motion opposite to the direction of the drive for a vacancy soliton. These two types of soliton behave as if they have opposite charges, and their direction of motion depends on their structure. For a quasi-1D sample, both the soliton and the skyrmion motion are strongly confined to the center axis of the sample by the repulsive barrier walls. It is also possible to induce soliton motion in 2D periodic lattices by providing a guiding channel in the form of a line of weak pinning centers. We show that the soliton motion is not strongly sensitive to the value of the skyrmion Hall angle, but that it is strongly affected by the pinning density. At low pinning densities the skyrmions are too far apart for collective behavior to appear and the soliton motion is destroyed. As the pinning density increases, the skyrmion-skyrmion interactions become relevant and a propagating soliton can be stabilized. When we vary α_m/α_d , we find that the soliton motion is the most prominent if the intrinsic skyrmion Hall angle is close to the soliton direction of motion. Nevertheless, even for angular differences as large as 90° , the soliton motion persists over a range of applied drives, indicating that the soliton phase is robust. In a sample where the skyrmion Hall angle is perpendicular to the weak pinning line, the soliton motion is aligned with the weak pinning at $+45^\circ$. As the external drive is increased, pinned skyrmions begin to depin and the skyrmion Hall angle

rotates from $+45^\circ$ to -45° in order to align with the intrinsic Hall angle. This indicates that at low drives the soliton motion can be guided, while for higher drives the skyrmions follow the intrinsic Hall angle. Such behavior is of interest for technological applications where the skyrmion motion must be controlled precisely and must follow directions different than the intrinsic skyrmion Hall angle. The moving soliton could be used as an information carrier in logic devices rather than the skyrmions themselves, making it possible to transport information at drives much lower than those needed to depin a chain of skyrmions. An advantage of this approach is that the solitons do not exhibit a finite skyrmion Hall angle.

ACKNOWLEDGMENTS

This work was supported by the U.S. Department of Energy through the Los Alamos National Laboratory. Los Alamos National Laboratory is operated by Triad National Security, LLC, for the National Nuclear Security Administration of U.S. Department of Energy (Contract No. 89233218CNA000001). Partial support from the Research Foundation-Flanders (FWO) and the Special Research Funds of the University of Antwerp (BOF) are gratefully acknowledged. N.P.V. acknowledges funding from Fundação de Amparo à Pesquisa do Estado de São Paulo - FAPESP (Grant No. 2017/20976-3). J.C.B.S. acknowledges funding from Fundação de Amparo à Pesquisa do Estado de São Paulo - FAPESP (Grant No. 2021/04941-0).

-
- [1] A. C. Scott, F. Y. F. Chu, and D. W. McLaughlin, The soliton: A new concept in applied science, *Proc. IEEE* **61**, 1443 (1973).
 - [2] N. J. Zabusky and M. D. Kruskal, Interaction of "Solitons" in a Collisionless Plasma and the Recurrence of Initial States, *Phys. Rev. Lett.* **15**, 240 (1965).
 - [3] S. Manukure and T. Booker, A short overview of solitons and applications, *Partial Differ. Eq. Appl. Math.* **4**, 100140 (2021).
 - [4] A. J. Heeger, S. Kivelson, J. R. Schrieffer, and W. P. Su, Solitons in conducting polymers, *Rev. Mod. Phys.* **60**, 781 (1988).
 - [5] L. M. Tolbert, Solitons in a box: The organic chemistry of electrically conducting polyenes, *Acc. Chem. Res.* **25**, 561 (1992).
 - [6] P. Ciblis and I. Cosic, The possibility of soliton/exciton transfer in proteins, *J. Theor. Biol.* **184**, 331 (1997).
 - [7] G.-P. Zhou, Biological functions of soliton and extra electron motion in DNA structure, *Phys. Scr.* **40**, 698 (1989).
 - [8] A. S. Davydov, The theory of contraction of proteins under their excitation, *J. Theor. Biol.* **38**, 559 (1973).
 - [9] A. Hasegawa and F. Tappert, Transmission of stationary nonlinear optical pulses in dispersive dielectric fibers. I. Anomalous dispersion, *Appl. Phys. Lett.* **23**, 142 (1973).
 - [10] L. F. Mollenauer, R. H. Stolen, and J. P. Gordon, Experimental Observation of Picosecond Pulse Narrowing and Solitons in Optical Fibers, *Phys. Rev. Lett.* **45**, 1095 (1980).
 - [11] G. C. Duree, J. L. Shultz, G. J. Salamo, M. Segev, A. Yariv, B. Crosignani, P. Di Porto, E. J. Sharp, and R. R. Neurgaonkar, Observation of Self-Trapping of an Optical Beam Due to the PhotoRefractive Effect, *Phys. Rev. Lett.* **71**, 533 (1993).
 - [12] W. E. Torruellas, Z. Wang, D. J. Hagan, E. W. VanStryland, G. I. Stegeman, L. Torner, and C. R. Menyuk, Observation of Two-Dimensional Spatial Solitary Waves in a Quadratic Medium, *Phys. Rev. Lett.* **74**, 5036 (1995).
 - [13] E. G. Galkina and B. A. Ivanov, Dynamic solitons in antiferromagnets (Review Article), *Low Temp. Phys.* **44**, 618 (2018).
 - [14] J. C. Slonczewski, Dynamics of magnetic domain walls, *AIP Conf. Proc.* **5**, 170 (1972).
 - [15] N. Papanicolaou and T. N. Tomaras, Dynamics of magnetic vortices, *Nucl. Phys. B* **360**, 425 (1991).
 - [16] A. M. Kosevich, B. A. Ivanov, and A. S. Kovalev, Magnon drops : A new type of collective excitations of ferromagnet, *J. Phys. Colloq.* **39**, C6-826 (1978).
 - [17] S. Mühlbauer, B. Binz, F. Jonietz, C. Pfleiderer, A. Rosch, A. Neubauer, R. Georgii, and P. Böni, Skyrmion lattice in a chiral magnet, *Science* **323**, 915 (2009).
 - [18] N. Nagaosa and Y. Tokura, Topological properties and dynamics of magnetic skyrmions, *Nat. Nanotechnol.* **8**, 899 (2013).
 - [19] F. Jonietz, S. Mühlbauer, C. Pfleiderer, A. Neubauer, W. Münzer, A. Bauer, T. Adams, R. Georgii, P. Böni, R. A. Duine *et al.*, Spin transfer torques in MnSi at ultralow current densities, *Science* **330**, 1648 (2010).
 - [20] T. Schulz, R. Ritz, A. Bauer, M. Halder, M. Wagner, C. Franz, C. Pfleiderer, K. Everschor, M. Garst, and A. Rosch, Emergent electrodynamics of skyrmions in a chiral magnet, *Nat. Phys.* **8**, 301 (2012).
 - [21] X. Z. Yu, N. Kanazawa, W. Z. Zhang, T. Nagai, T. Hara, K. Kimoto, Y. Matsui, Y. Onose, and Y. Tokura, Skyrmion flow

- near room temperature in an ultralow current density, *Nat. Commun.* **3**, 988 (2012).
- [22] J. Iwasaki, M. Mochizuki, and N. Nagaosa, Universal current-velocity relation of skyrmion motion in chiral magnets, *Nat. Commun.* **4**, 1463 (2013).
- [23] S.-Z. Lin, C. Reichhardt, C. D. Batista, and A. Saxena, Driven Skyrmions and Dynamical Transitions in Chiral Magnets, *Phys. Rev. Lett.* **110**, 207202 (2013).
- [24] D. Liang, J. P. DeGrave, M. J. Stolt, Y. Tokura, and S. Jin, Current-driven dynamics of skyrmions stabilized in MnSi nanowires revealed by topological Hall effect, *Nat. Commun.* **6**, 8217 (2015).
- [25] S. Woo, K. Litzius, B. Krüger, Mi-Young Im, L. Caretta, K. Richter, M. Mann, A. Krone, R. M. Reeve, M. Weigand *et al.*, Observation of room-temperature magnetic skyrmions and their current-driven dynamics in ultrathin metallic ferromagnets, *Nat. Mater.* **15**, 501 (2016).
- [26] A. Fert, V. Cros, and J. Sampaio, Skyrmions on the track, *Nat. Nanotechnol.* **8**, 152 (2013).
- [27] A. Fert, N. Reyren, and V. Cros, Magnetic skyrmions: Advances in physics and potential applications, *Nat. Rev. Mater.* **2**, 1 (2017).
- [28] R. Wiesendanger, Nanoscale magnetic skyrmions in metallic films and multilayers: A new twist for spintronics, *Nat. Rev. Mater.* **1**, 1 (2016).
- [29] J. Iwasaki, M. Mochizuki, and N. Nagaosa, Current-induced skyrmion dynamics in constricted geometries, *Nat. Nanotechnol.* **8**, 742 (2013).
- [30] X. Z. Yu, Y. Onose, N. Kanazawa, J. H. Park, J. H. Han, Y. Matsui, N. Nagaosa, and Y. Tokura, Real-space observation of a two-dimensional skyrmion crystal, *Nature (London)* **465**, 901 (2010).
- [31] W. Jiang, X. Zhang, G. Yu, W. Zhang, X. Wang, M. B. Jungfleisch, J. E. Pearson, X. Cheng, O. Heinonen, K. L. Wang *et al.*, Direct observation of the skyrmion Hall effect, *Nat. Phys.* **13**, 162 (2017).
- [32] K. Zeissler, S. Finizio, C. Barton, A. J. Huxtable, J. Massey, J. Raabe, A. V. Sadovnikov, S. A. Nikitov, R. Brearton, T. Hesjedal *et al.*, Diameter-independent skyrmion Hall angle observed in chiral magnetic multilayers, *Nat. Commun.* **11**, 428 (2020).
- [33] K. Litzius, I. Lemesch, B. Krüger, P. Bassirian, L. Caretta, K. Richter, F. Büttner, K. Sato, O. A. Tretiakov, J. Förster *et al.*, Skyrmion Hall effect revealed by direct time-resolved x-ray microscopy, *Nat. Phys.* **13**, 170 (2017).
- [34] Y. Zhang, S. Luo, B. Yan, J. Ou-Yang, X. Yang, S. Chen, B. Zhu, and L. You, Magnetic skyrmions without the skyrmion Hall effect in a magnetic nanotrack with perpendicular anisotropy, *Nanoscale* **9**, 10212 (2017).
- [35] C. Reichhardt, D. Ray, and C. J. Olson Reichhardt, Quantized transport for a skyrmion moving on a two-dimensional periodic substrate, *Phys. Rev. B* **91**, 104426 (2015).
- [36] N. P. Vizarim, C. J. Olson Reichhardt, P. A. Venegas, and C. Reichhardt, Skyrmion dynamics and transverse mobility: Skyrmion Hall angle reversal on 2D periodic substrates with dc and biharmonic ac drives, *Eur. Phys. J. B* **93**, 112 (2020).
- [37] N. P. Vizarim, C. J. Olson Reichhardt, P. A. Venegas, and C. Reichhardt, Skyrmion pinball and directed motion on obstacle arrays, *J. Phys. Commun.* **4**, 085001 (2020).
- [38] J. Feilhauer, S. Saha, J. Tobik, M. Zelent, L. J. Heyderman, and M. Mruzckiewicz, Controlled motion of skyrmions in a magnetic antidot lattice, *Phys. Rev. B* **102**, 184425 (2020).
- [39] N. P. Vizarim, J. C. Bellizotti Souza, C. Reichhardt, C. J. Olson Reichhardt, and P. A. Venegas, Directional locking and the influence of obstacle density on skyrmion dynamics in triangular and honeycomb arrays, *J. Phys.: Condens. Matter* **33**, 305801 (2021).
- [40] D. Stosic, T. B. Ludermit, and M. V. Milošević, Pinning of magnetic skyrmions in a monolayer Co film on Pt(111): Theoretical characterization and exemplified utilization, *Phys. Rev. B* **96**, 214403 (2017).
- [41] C. Reichhardt and F. Nori, Phase Locking, Devil's Staircases, Farey Trees, and Arnold Tongues in Driven Vortex Lattices with Periodic Pinning, *Phys. Rev. Lett.* **82**, 414 (1999).
- [42] T. Bohlein and C. Bechinger, Experimental Observation of Directional Locking and Dynamical Ordering of Colloidal Monolayers Driven across Quasiperiodic Substrates, *Phys. Rev. Lett.* **109**, 058301 (2012).
- [43] C. Reichhardt and C. J. Olson Reichhardt, Directional locking effects and dynamics for particles driven through a colloidal lattice, *Phys. Rev. E* **69**, 041405 (2004).
- [44] A. Gopinathan and D. G. Grier, Statistically Locked-In Transport through Periodic Potential Landscapes, *Phys. Rev. Lett.* **92**, 130602 (2004).
- [45] N. P. Vizarim, C. Reichhardt, C. J. Olson Reichhardt, and P. A. Venegas, Skyrmion dynamics and topological sorting on periodic obstacle arrays, *New J. Phys.* **22**, 053025 (2020).
- [46] C. Reichhardt, D. Ray, and C. J. Olson Reichhardt, Nonequilibrium phases and segregation for skyrmions on periodic pinning arrays, *Phys. Rev. B* **98**, 134418 (2018).
- [47] W. Chen, L. Liu, Y. Ji, and Y. Zheng, Skyrmion ratchet effect driven by a biharmonic force, *Phys. Rev. B* **99**, 064431 (2019).
- [48] B. Göbel and I. Mertig, Skyrmion ratchet propagation: Utilizing the skyrmion Hall effect in AC racetrack storage devices, *Sci. Rep.* **11**, 3020 (2021).
- [49] X. Ma, C. J. Olson Reichhardt, and C. Reichhardt, Reversible vector ratchets for skyrmion systems, *Phys. Rev. B* **95**, 104401 (2017).
- [50] C. Reichhardt, D. Ray, and C. J. Olson Reichhardt, Magnus-induced ratchet effects for skyrmions interacting with asymmetric substrates, *New J. Phys.* **17**, 073034 (2015).
- [51] J. C. Bellizotti Souza, N. P. Vizarim, C. J. O. Reichhardt, C. Reichhardt, and P. A. Venegas, Skyrmion ratchet in funnel geometries, *Phys. Rev. B* **104**, 054434 (2021).
- [52] R. Yamaguchi, K. Yamada, and Y. Nakatani, Control of current-induced skyrmion motion in ratchet-type skyrmion-based racetrack memory with a loop structure, *Jpn. J. Appl. Phys.* **60**, 010904 (2020).
- [53] N. P. Vizarim, C. Reichhardt, P. A. Venegas, and C. J. O. Reichhardt, Guided skyrmion motion along pinning array interfaces, *J. Magn. Magn. Mater.* **528**, 167710 (2021).
- [54] C.-L. Zhang, J.-N. Wang, C.-K. Song, N. Mehmood, Z.-Z. Zeng, Y.-X. Ma, J.-B. Wang, and Q.-F. Liu, Edge-guided heart-shaped skyrmion, *Rare Metals* **41**, 865 (2022).
- [55] R. Yanes, F. Garcia-Sanchez, R. F. Luis, E. Martinez, V. Raposo, L. Torres, and L. Lopez-Diaz, Skyrmion motion induced by voltage-controlled in-plane strain gradients, *Appl. Phys. Lett.* **115**, 132401 (2019).

- [56] S. L. Zhang, W. W. Wang, D. M. Burn, H. Peng, H. Berger, A. Bauer, C. Pfeleiderer, G. van der Laan, and T. Hesjedal, Manipulation of skyrmion motion by magnetic field gradients, *Nat. Commun.* **9**, 2115 (2018).
- [57] A. Casiraghi, H. Corte-León, M. Vafaee, F. Garcia-Sanchez, G. Durin, M. Pasquale, G. Jakob, M. Kläui, and O. Kazakova, Individual skyrmion manipulation by local magnetic field gradients, *Commun. Phys.* **2**, 1 (2019).
- [58] K. Everschor, M. Garst, B. Binz, F. Jonietz, S. Mühlbauer, C. Pfeleiderer, and A. Rosch, Rotating skyrmion lattices by spin torques and field or temperature gradients, *Phys. Rev. B* **86**, 054432 (2012).
- [59] L. Kong and J. Zang, Dynamics of an Insulating Skyrmion under a Temperature Gradient, *Phys. Rev. Lett.* **111**, 067203 (2013).
- [60] Y. Wang, T. Shimada, J. Wang, T. Kitamura, and H. Hirakata, The rectilinear motion of the individual asymmetrical skyrmion driven by temperature gradients, *Acta Mater.* **221**, 117383 (2021).
- [61] I. Purnama, W. L. Gan, D. W. Wong, and W. S. Lew, Guided current-induced skyrmion motion in 1D potential well, *Sci. Rep.* **5**, 10620 (2015).
- [62] R. Juge, K. Bairagi, K. G. Rana, J. Vogel, M. Sall, D. Mailly, V. T. Pham, Q. Zhang, N. Sisodia, M. Foerster *et al.*, Helium ions put magnetic skyrmions on the track, *Nano Lett.* **21**, 2989 (2021).
- [63] J. Leliaert, P. Gypens, M. V. Milošević, B. Van Waeyenberge, and J. Mulkers, Coupling of the skyrmion velocity to its breathing mode in periodically notched nanotracks, *J. Phys. D* **52**, 024003 (2018).
- [64] X. Zhang, Y. Zhou, M. Ezawa, G. P. Zhao, and W. Zhao, Magnetic skyrmion transistor: Skyrmion motion in a voltage-gated nanotrack, *Sci. Rep.* **5**, 11369 (2015).
- [65] X. Chen, W. Kang, D. Zhu, X. Zhang, N. Lei, Y. Zhang, Y. Zhou, and W. Zhao, Skyrmion dynamics in width-varying nanotracks and implications for skyrmionic applications, *Appl. Phys. Lett.* **111**, 202406 (2017).
- [66] D. Toscano, J. P. A. Mendonça, A. L. S. Miranda, C. I. L. de Araujo, F. Sato, P. Z. Coura, and S. A. Leonel, Suppression of the skyrmion Hall effect in planar nanomagnets by the magnetic properties engineering: Skyrmion transport on nanotracks with magnetic strips, *J. Magn. Magn. Mater.* **504**, 166655 (2020).
- [67] R. M. Menezes, J. F. S. Neto, C. C. deSouza Silva, and M. V. Milošević, Manipulation of magnetic skyrmions by superconducting vortices in ferromagnet-superconductor heterostructures, *Phys. Rev. B* **100**, 014431 (2019).
- [68] U. Welp, Z. L. Xiao, V. Novosad, and V. K. Vlasko-Vlasov, Commensurability and strong vortex pinning in nanopatterned Nb films, *Phys. Rev. B* **71**, 014505 (2005).
- [69] C. Reichhardt, C. J. Olson, and Franco Nori, Commensurate and incommensurate vortex states in superconductors with periodic pinning arrays, *Phys. Rev. B* **57**, 7937 (1998).
- [70] K. Harada, O. Kamimura, H. Kasai, T. Matsuda, A. Tonomura, and V. V. Moshchalkov, Direct observation of vortex dynamics in superconducting films with regular arrays of defects, *Science* **274**, 1167 (1996).
- [71] K. Mangold, P. Leiderer, and C. Bechinger, Phase Transitions of Colloidal Monolayers in Periodic Pinning Arrays, *Phys. Rev. Lett.* **90**, 158302 (2003).
- [72] D. G. Rees, H. Totsuji, and K. Kono, Commensurability-Dependent Transport of a Wigner Crystal in a Nanoconstriction, *Phys. Rev. Lett.* **108**, 176801 (2012).
- [73] H. Pu, L. O. Baksmaty, S. Yi, and N. P. Bigelow, Structural Phase Transitions of Vortex Matter in an Optical Lattice, *Phys. Rev. Lett.* **94**, 190401 (2005).
- [74] S. Tung, V. Schweikhard, and E. A. Cornell, Observation of Vortex Pinning in Bose-Einstein Condensates, *Phys. Rev. Lett.* **97**, 240402 (2006).
- [75] A. Duzgun, C. Nisoli, C. J. O. Reichhardt, and C. Reichhardt, Commensurate states and pattern switching via liquid crystal skyrmions trapped in a square lattice, *Soft Matter* **16**, 3338 (2020).
- [76] C. Reichhardt and C. J. O. Reichhardt, Commensuration effects on skyrmion Hall angle and drag for manipulation of skyrmions on two-dimensional periodic substrates, [arXiv:2202.00766](https://arxiv.org/abs/2202.00766).
- [77] T. A. Kontorova and Y. I. Fraenkel, On the theory of plastic deformation and twinning, *Zh. Eksp. Teor. Fiz.* **8**, 89 (1938).
- [78] O. M. Braun and Y. S. Kivshar, Nonlinear dynamics of the Frenkel-Kontorova model, *Phys. Rep.* **306**, 1 (1998).
- [79] J. Tekić, O. M. Braun, and B. Hu, Dynamic phases in the two-dimensional underdamped driven Frenkel-Kontorova model, *Phys. Rev. E* **71**, 026104 (2005).
- [80] T. Bohlein, J. Mikhael, and C. Bechinger, Observation of kinks and antikinks in colloidal monolayers driven across ordered surfaces, *Nat. Mater.* **11**, 126 (2012).
- [81] A. Vanossi, N. Manini, and E. Tosatti, Static and dynamic friction in sliding colloidal monolayers, *Proc. Natl. Acad. Sci. USA* **109**, 16429 (2012).
- [82] A. Benassi, A. Vanossi, and E. Tosatti, Nanofriction in cold ion traps, *Nat. Commun.* **2**, 236 (2011).
- [83] A. Vanossi, N. Manini, M. Urbakh, S. Zapperi, and E. Tosatti, Colloquium: Modeling friction: From nanoscale to mesoscale, *Rev. Mod. Phys.* **85**, 529 (2013).
- [84] A. Vanossi, C. Bechinger, and M. Urbakh, Structural lubricity in soft and hard matter systems, *Nat. Commun.* **11**, 4657 (2020).
- [85] C. Reichhardt and C. J. Olson, Depinning and nonequilibrium dynamic phases of particle assemblies driven over random and ordered substrates: A review, *Rep. Prog. Phys.* **80**, 026501 (2017).
- [86] S.-Z. Lin, C. Reichhardt, C. D. Batista, and A. Saxena, Particle model for skyrmions in metallic chiral magnets: Dynamics, pinning, and creep, *Phys. Rev. B* **87**, 214419 (2013).
- [87] J. Zang, M. Mostovoy, J. H. Han, and N. Nagaosa, Dynamics of Skyrmion Crystals in Metallic Thin Films, *Phys. Rev. Lett.* **107**, 136804 (2011).